Çukurova Üniversitesi
Mühendislik Fakültesi Dergisi
Çukurova University
Journal of the Faculty of Engineering

ISSN: 2757-9255 CİLT/VOLUME: 40 SAYI/ISSUE: 4 ARALIK/DECEMBER 2025

A Comparative Experimental Analysis of Flexural Performance of Stainless Steel and CFRP Bone Plates under Four-Point Bending

Ahmet ÇETİN [1,a]

[1]*Alanya Alaaddin Keykubat University, Rafet Kayış Engineering Faculty, Department of Mechanical Engineering, Alanya, Türkiye*

[a]***ORCID**: 0000-0003-1393-3806*

Article Info

Received : 25.08.2025
Accepted : 20.11.2025
DOI: 10.21605/cukurovaumfd.1772159

Corresponding Author

Ahmet ÇETİN
ahmet.cetin@alanya.edu.tr

Keywords

CFRP bone plates
316L stainless steel bone plates
Four-point bending
Stiffness-to-weight ratio

***How to cite:** ÇETİN, A., (2025). A Comparative Experimental Analysis of Flexural Performance of Stainless Steel and CFRP Bone Plates under Four-Point Bending. Cukurova University, Journal of the Faculty of Engineering, 40(4), 915-925.*

ABSTRACT

Metal bone plates are one of the most common clinical applications for fracture fixation; however, optimization of the stiffness-to-weight ratio is often overlooked. This study compared 316L stainless steel plates and lightweight carbon fiber-reinforced polymer (CFRP) plates of identical geometry. The plates were tested using the standard four-point bending test in both short and long configurations. Stiffness and bending moment parameters were obtained from load-displacement curves, and specific stiffness and specific moment were also determined. CFRP plates demonstrated higher specific bending stiffness, while steel exhibited higher absolute stiffness. The short CFRP plate exhibited reduced stiffness attributable to a net loss of cross-sectional area near the hole. The mechanical findings suggest that CFRP is a suitable material for designs that prioritize stiffness-to-mass performance, particularly in elongated plates when the connection-element region is considered a primary design feature.

Dört Noktadan Bükülme Altında Paslanmaz Çelik ve CFRP Kemik Plakalarının Eğilme Performansının Karşılaştırmalı Deneysel Analizi

Makale Bilgileri

Geliş : 25.08.2025
Kabul : 20.11.2025
DOI: 10.21605/cukurovaumfd.1772159

Sorumlu Yazar

Ahmet ÇETİN
ahmet.cetin@alanya.edu.tr

Anahtar Kelimeler

CFRP kemik plakaları
316L paslanmaz çelik kemik plakaları
Dört noktadan bükülme
Sertlik-ağırlık oranı

***Atıf şekli:** ÇETİN, A., (2025). Dört Noktadan Bükülme Altında Paslanmaz Çelik ve CFRP Kemik Plakalarının Eğilme Performansının Karşılaştırmalı Deneysel Analizi. Çukurova Üniversitesi, Mühendislik Fakültesi Dergisi, 40(4), 915-925.*

ÖZ

Metalik kemik plakaları, kırık sabitlemesi için en yaygın klinik uygulamalardan biridir, ancak rijitlik-ağırlık oranının optimizasyonunu göz ardı edilmektedir. Bu çalışmada, aynı geometriye sahip 316L paslanmaz çelik ve hafif yapılı karbon fiber takviyeli polimer (CFRP) plakaların karşılaştırılmasına odaklanılmıştır. Plakalar hem kısa hem de uzun konfigürasyonlarda dört noktalı eğilme standardı altında test edilmiştir. Rijitlik ve eğilme momenti parametreleri yük-sehim eğrilerinden elde edilmiş, ayrıca özgül moment ve özgül rijitlik de belirlenmiştir. CFRP plakalar daha yüksek özgül eğilme rijitliği gösterirken, çelik daha yüksek mutlak rijitlik sergilemiştir. Kısa CFRP plaka ise, deliğin yakınındaki net kesit kaybına bağlı olarak daha düşük rijitlik göstermiştir. Mekanik bulgular, CFRP'nin, özellikle bağlantı elemanı bölgesi birincil tasarım özelliği olarak kabul edildiğinde, rijitlik-kütle performansını önceliklendiren tasarımlar için, özellikle uzun plakalarda uygun bir malzeme olduğunu göstermektedir.

1. INTRODUCTION

In contemporary medical practice, the use of internal and external orthopedic implants has become a prevalent approach to managing trauma-related fractures and surgical interventions, such as bone lengthening [1]. Ring fixators, rods, and V-frames are external fixators, while bone plates, pins, and screws are internal fixators [2]. Despite their seemingly simple design, bone plates are among the most frequently used internal fixation devices in orthopedics, reflecting their broad range of clinical applications [3]. These devices are commonly used in the treatment of fractures of long bones, including the femur, tibia, and ulna, as well as fractures of the small bones of the fingers. [4]. The diversity of their applications is illustrated in Figure 1.

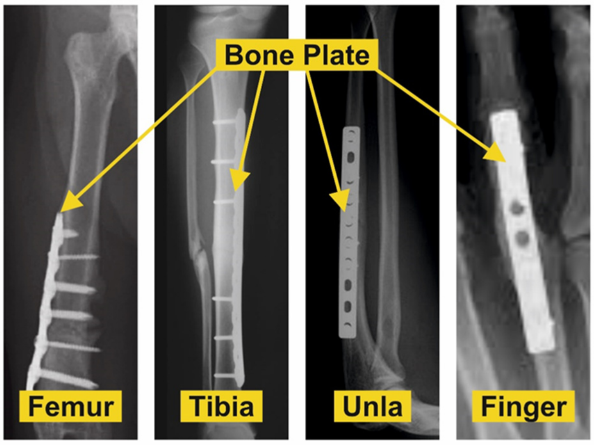

Figure 1. Example X-ray images of broken bones fixed with bone plates

The dimensions of bone plates (i.e., thickness, width, and length) are determined by the intended application [5]. A standard design configuration consists of a rectangular cross-section, with bone screw holes, and short and long variants. This configuration is intended to enhance bending stiffness during load transfer, while concurrently constraining stress concentrations around the screw holes [6]. In comparative evaluations, four-point bending is widely used to characterize plate behavior because the constant-moment region minimizes shear effects, enabling reliable assessment under bending loads [7-11]. Preliminary research has demonstrated that plate thickness, plate width, and plate type have a substantial impact on bending stiffness and strength. This establishes stiffness as a primary design parameter [12-17]. Material selection also constitutes a pivotal implant design parameter, as does dimensional design [18,19]. The selection of materials is typically predicated on a multifaceted set of criteria, including biocompatibility (ISO 10993), corrosion and fatigue resistance, mechanical compatibility, and imaging compatibility [19-21]. In contemporary applications, stainless steel (AISI 316L), titanium, and titanium-aluminum alloys are frequently utilized [18,19]. However, these materials have both advantages and disadvantages. Titanium and Ti–6Al–4V have been demonstrated to exhibit superior corrosion resistance and high imaging compatibility [19,22,23]. However, stainless steel is advantageous when the priorities are cost, formability, and high yield strength [19,21,22].

However, studies directly examining the performance of bone plates produced from these materials have been limited to investigations of bending stiffness or bending moment. Evaluations establishing the mass-stiffness relationship and density-normalized comparisons between materials are particularly inadequate. A frequently overlooked aspect in bone plate design is the stiffness-to-weight ratio. Historically, the primary design criteria have centered on dimensional and material compatibility. In contrast, the need to achieve the desired stability without unnecessary increases in mass has been of secondary importance. In this relationship, composite materials, which have become increasingly prevalent over the past half-century due to their low densities, mechanically tunable properties resulting from fiber orientation, and high specific performance, are beginning to replace traditional materials [24,25]. These materials have become popular choices for a wide range of engineering applications, including aerospace, automotive, military, and marine industries [2,26-31]. Despite their limited use relative to other applications, interest in their use in biomedical use has emerged [2,32,33]. Specifically, the capacity to modify the elastic modulus of these materials to a range approaching that of bone can mitigate the risk of stress shielding during stabilization [32,34]. Regarding patient comfort, a reduction in implant mass has been shown to decrease the weight-bearing load and fatigue experienced during activities of daily living [35,36]. Furthermore, their radiolucent properties prevent overlap between bone and implant boundaries in X-ray images, and reduced MR/CT artifacts improve image quality during surgical planning and postoperative follow-up [37,38]. Consequently, there has been growing interest in studying carbon-fiber composite bone plates [33,37]. However, studies directly examining the performance of bone plates made from these materials are limited, and comparisons conducted under mass-normalized evaluations and geometric controls are particularly lacking.

Accordingly, the objective of this study is to compare the mechanical performance of bone plates made from 316L stainless steel and carbon-fiber-reinforced polymer (CFRP) under standardized four-point bending tests. To ensure a material-focused comparison, the hole pattern and hole-size geometry were held constant across all configurations, thereby controlling design variables that would complicate the comparisons between materials. In order to enhance the generalizability of the findings, only two distinct plate lengths were added as a secondary design factor. To overcome the limitations of traditional evaluations, a set of metrics was collected. This array included not only absolute bending results but also mass-normalized indicators, such as specific stiffness and specific bending capacity. Consequently, stability was also assessed with respect to specific performance. The evidence obtained will support designers' decisions when selecting materials that balance absolute stability and stiffness efficiency, especially in applications where implant mass is critical. The study will provide a substantial reference framework for weight-sensitive bone-plate designs.

2. MATERIALS AND METHODS

2.1. Stainless Steel Bone Plate

A simple dynamic compression plate (DCP) style, which has a rectangular cross-section and standard hole spacing, was selected to investigate solely the material effect within the same geometry. This choice ensured a fair, reproducible, and comparable benchmark by eliminating the confounding effects of design elements such as specific locking interfaces and reduced bottom contact surfaces, as well as process deviations in composite manufacturing. Long and short stainless-steel DCP bone plates were purchased from Hipokrat Medical Materials Manufacturing and Marketing, Inc. All geometric and dimensional data reported in this study (overall lengths, widths, thicknesses, hole diameters, and hole pitches) were determined exclusively by direct measurements of the test specimens using a digital caliper (0.01 mm resolution) and a micrometer. The dimensions of the long plates are 200 mm in length, 16 mm in width, and 4 mm in thickness. The holes are arranged in a cross-shaped configuration on the plate, totaling 12 slotted holes. The holes were measured and found to have diameters of 6 mm and center-to-center distances of 3 mm. The dimensions of the short plates are 150 mm in length, 16 mm in width, and 4 mm in thickness. The plate exhibits a total of 12 holes, including four outer holes, each with a diameter of 7 mm and five inner holes, each with a diameter of 5 mm. These holes are arranged in a cross pattern. The plates used in the study are shown in Figure 2.

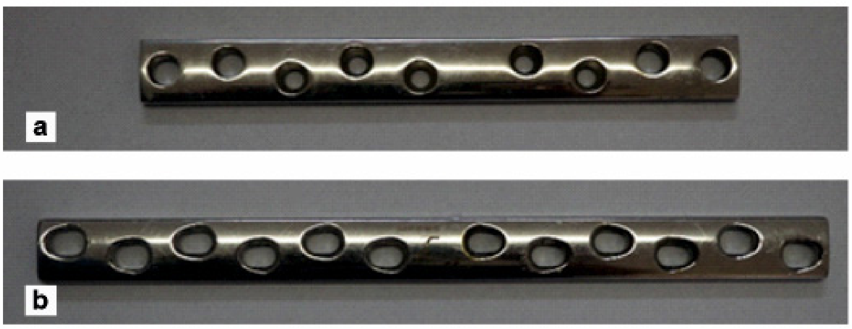

Figure 2. DCP stainless steel bone plates obtained from Hipokrat Medical Materials Manufacturing and Marketing Inc.; a) short plate, b) long plate

2.2. Manufacturing of Composite Bone Plate

The production of composite plates was carried out in detail, encompassing the initial material preparation through the final inspection steps, in accordance with the process shown in Figure 3. First, plain-woven carbon fabrics (300 g/m², 3K) were cut into 250 × 200 mm and 200 × 200 mm pieces without disrupting the fiber orientation of the main sheets, from which short and long plates were obtained. A total of 20 layers were planned to achieve a 4 mm thickness on the steel plates. The matrix was prepared by mixing the MGS Laminating Epoxy Set L160/H160 at the specified ratio of 100:25, using low speed to minimize air bubble formation. The fabrics were impregnated with resin and stacked on a waxed glass surface, covered with a perforated release film and a breather, and sealed in a vacuum bag. The stack was cured under a vacuum of 1 atm at 25 °C for 24 hours, after which the panel was removed from the mold (see Figure 3a). The final dimensions of 200 × 16 mm and 150 × 16 mm were achieved on a vertical cutting bench. A backing material was used during cutting to prevent edge delamination (Figure 3b). Then, on a vertical drilling bench, screw holes were drilled at specified diameters with appropriate countersink widths and aligned with the plate geometry. The hole diameter, position, and surface quality were inspected (Figure 3c). After completing these steps, composite plates with the same dimensions and hole layout as the flat stainless-steel plates were obtained (Figure 3d).

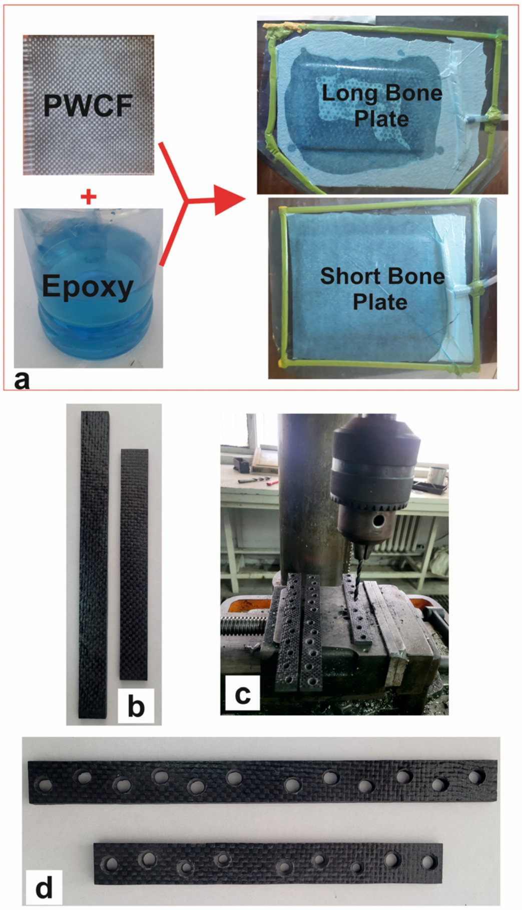

Figure 3. Production process of composite bone plates: a) vacuum production, b) plates cut to length and width, c) drilling of screw holes, d) finished bone plates

2.3. Four-point Bending Tests of Bone Plates

Four-point bending tests were conducted in accordance with ASTM F382 [39] and under displacement control. Figure 4a shows the standard schematic layout, and Figures 4b and 4c show representative layouts of metallic and composite short- and long-plate specimens. For ease of reading, the short stainless-steel bone plate (SSBP), long stainless-steel bone plate (LSBP), short composite bone plate (SCBP), and long composite bone plate (LCBP) were coded. Since ASTM F382 does not specify a fixed crosshead speed, a loading speed of 1.0 mm/min was selected according to the composite bending standard ASTM D7264/D7264M to account for the polymer-matrix composite nature of some samples and to control speed-sensitivity effects (viscoelasticity). Three replicates were performed for each sample type (short metal, long metal, short composite, and long composite), resulting in a total of 12 tests. The tests were conducted at room temperature. In the four-point bending fixture, the lower opening, L, was set to 100 mm for the short group and 140 mm for the long group. The load–support distance (h) was determined based on the L/3 principle for each group. Accordingly, h ≈ 33.3 mm for the short group and h ≈ 46.7 mm for the long group. The center spacing a between the upper loading cylinders was kept the same for both groups and set at approximately 34 mm to account for production tolerances. During loading, displacement data at the loading point were recorded continuously. Loading continued until the linear region was sufficiently sampled to reliably calculate the proof load. Then the samples were loaded until the intersection of the F–u curve and the offset line was reached or damage or failure occurred. Proof load (P_{proof}) is defined as the load at the intersection of the experimental curve and the linear fit, determined using the 0.2% offset specified in the standard. If the sample is damaged before the intersection occurs, Fmax is reported.

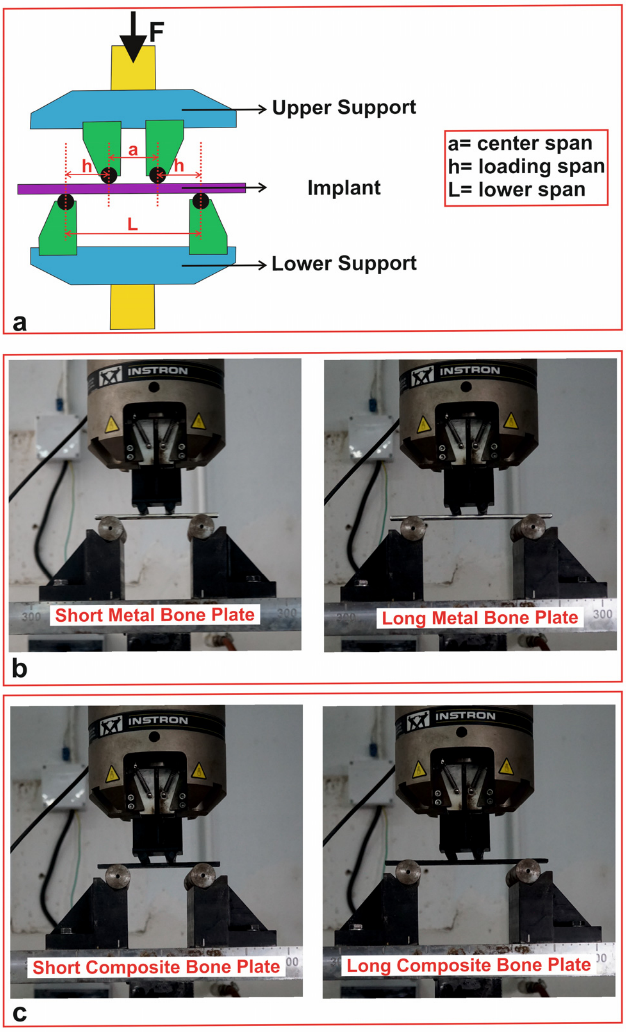

Figure 4. Four-point bending test setup and test specimens according to ASTM F382. a) Test schematic; b) SSBP and LSBP; c) SCBP and LCBP test configuration

Calculations were performed in accordance with ASTM F382 [39]. Bending stiffness (K) is obtained as the slope of the linear-elastic portion of the load–displacement curve (F–u): K = dF/du (N/mm). The bending moment in the constant-moment region was included in the calculation using the equation $M = (P \cdot h)/2$; normally $P = P_{proof,}$ while in the case of failure $P = F_{max}$. Equivalent structural bending stiffness (EI) was calculated using Equation 1 for four-point bending geometry. In this study, density normalization was performed based on the values obtained according to the standard F382. Using the concept of density normalization, the "specific bending stiffness," and "specific moment capacity" were calculated as EI/ρ and M/ρ, respectively.

$$EI = \frac{(2h+3a)Kh^2}{12} \tag{1}$$

Symbols and units used in Equation (1) are: h (mm), load-support distance; a (mm), center-to-center spacing of the upper loading cylinders; K (N/mm), elastic stiffness. Analyses were performed on K, M, and EI obtained from four-point bending and, on their density, normalized counterparts (K/ρ, M/ρ and EI/ρ). Given that the design was balanced (n = 3 per cell), a two-way fixed-effects ANOVA was employed, with factors material (316L vs. CFRP) and length (short vs. long). The validity of the model assumptions was assessed by examining the residuals (Shapiro–Wilk for normality; Brown–Forsythe/Levene for homogeneity of variance). In instances where the assumptions were deemed invalid, a monotonic variance-stabilizing transformation (e.g., Box–Cox) was considered. When the omnibus test indicated significance, post hoc pairwise comparisons were conducted on estimated marginal means, with Tukey's HSD adjustment to control the family-wise error rate (Tukey–Kramer when group sizes/variances differed). The effect sizes were reported as partial η^2 for analysis of variance (ANOVA) and Hedges' g for paired comparisons, both with 95% confidence intervals (bootstrapped where appropriate). Unless stated otherwise, data are presented as mean ± SD. The significance level was set at $\alpha = 0.05$.

3. RESULT AND DISCUSSION

The F–u curves displayed in Figure 5 demonstrate a discernible initial elastic, linear phase and variations in the material, or clearance-induced slope across all four-point bending test configurations. The slope is steeper in steel specimens than those in CFRP, and shorter plates exhibit higher slope values than longer ones. Regarding the load criterion (see Figure 5), the P_{proof} value, defined as the 0.2% offset, was attained for the SSBP and LSBP specimens. However, due to the brittle nature of CFRP, the SCBP and LCBP specimens fractured in the linear region without reaching the elastic limit. Consequently, Fmax was used in the results instead of P_{proof} for these plates.

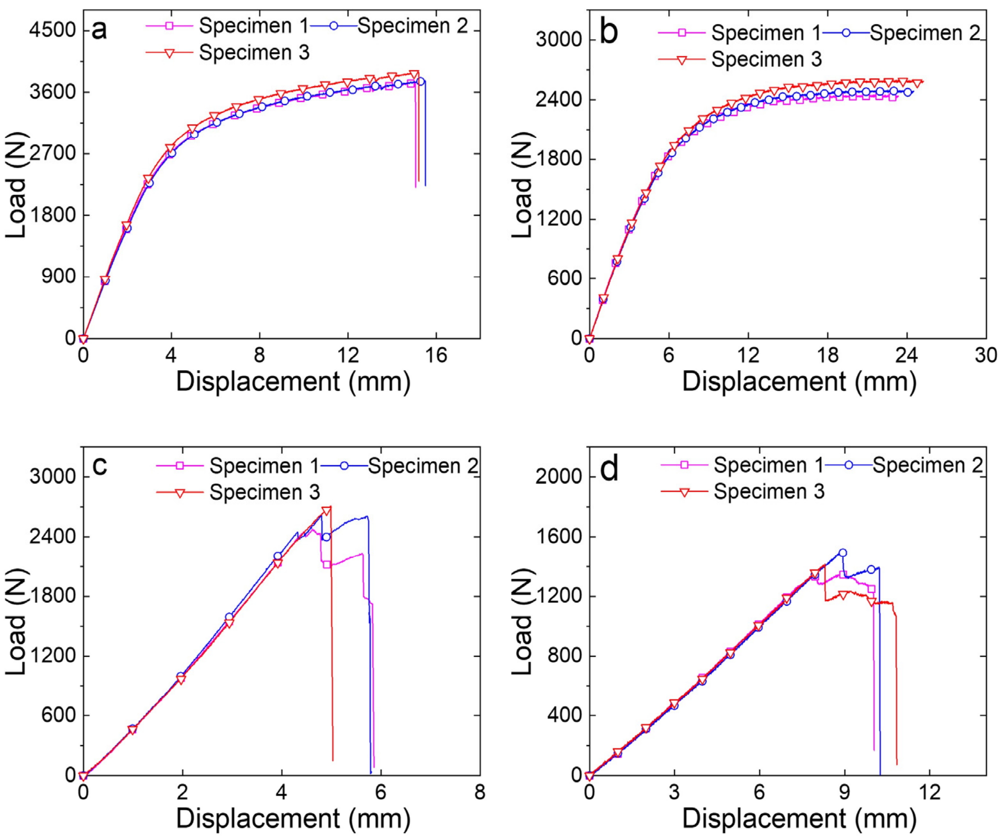

Figure 5. Force-displacement curves a) SSBP, b) LSBP, c) SCBP, d) LCBP

Table 1. Results calculated from the tests conducted and the data obtained in the study

Configuration		SSBP	SCBP	LSBP	LCBP
Force type	-	P_{proof}	F_{max}	P_{proof}	F_{max}
Force	P/F (N)	1511 ± 20	2599 ± 95	1019 ± 17	1423 ± 64
Bending rigidity	K (N/mm)	866 ± 18	600 ± 9	377 ± 4	179 ± 2
Bending moment	M (N.mm)	25180 ± 336	43323 ± 1591	23793 ± 409	33205 ±1510
Equivalent bending rigidity	EI (N.mm²)	13530176 ± 286332	9373851 ± 153555	13385692 ± 149484	6347744 ± 101129
Density	ρ (g/mm³)	0.008	0.001486	0.008	0.001486
Specific K	K/ρ (N.mm²/g)	108320 ± 2292	404015 ± 6618	47191 ± 527	120480 ± 1919
Specific M	M/ρ (N.mm⁴/g)	3147601 ± 42111	29154404 ± 1071234	2974240 ± 51209	22345696 ± 1016796
Specific EI	EI/ρ (N.mm⁵/g)	1691272042 ± 35791562	6308109731 ± 103334609	1673211553 ± 18685604	4271698845 ± 68055046

It is imperative to evaluate the rigidity and moment findings in conjunction with Figures 6b and 6c and Table 1. Two-way ANOVA with Tukey-adjusted pairwise comparisons showed significant main effects of material and length on K and M (steel exhibited greater absolute stiffness than CFRP; increasing length reduced K but increased M in both materials). For density-normalized metrics, a significant material-by-length interaction was observed: both CFRP configurations exceeded steel in K/ρ, M/ρ, and EI/ρ, and SCBP exceeded LCBP for all three metrics (all $p < 0.05$; see Figure 7 and Table 1). The increase in span length, despite the increase in the constant moment arm, has led to a reduction in K by approximately 31% (from 866 to 600 N/mm) in steel and by approximately 53% (from 377 to 179 N/mm) in CFRP, owing to the increased beam deflection. Concurrently, M has increased by approximately 72% (from 25,180 to 43,323 N.mm) in steel and by approximately 40% (from 23,793 to 33,205 N.mm) in CFRP, due to the augmented moment arm. The steel-to-CFRP hierarchy is maintained within the same span class, exhibiting a stiffness ratio of approximately 2.30 for short plates and approximately 3.35 for long plates. These results align with the rankings exhibited in Figures 6b and 6c and with the slope- and moment-based interpretations of the F–u curves.

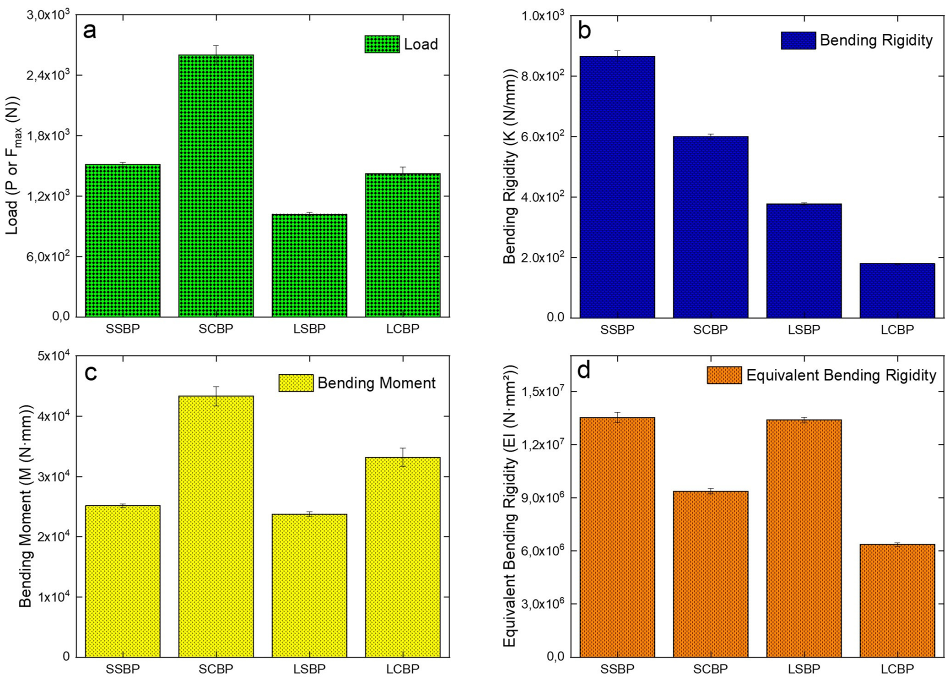

Figure 6. Raw metrics for four-point bending, a) load criterion, b) bending stiffness, c) bending moment, and d) equivalent bending stiffness. Bars show mean ± SD (n = 3). Distinct letters denote significant differences at p 0.05

As illustrated in Figure 6d, a critical distinction in equivalent bending stiffness (EI) is emphasized. While SSBP and LSBP align with anticipated trends, LCBP demonstrates a reduced absolute elastic inertia (EI) compared to steel plates. However, subsequent analysis will illustrate that LCBP exhibits a substantial advantage when mass-normalized. The low EI of LCBP is primarily span-driven (greater compliance at longer working length), whereas in the short CFRP configuration, local hole proximity and ply architecture can reduce EI relative to steel without indicating a material weakness. In plain-weave (0°/90°) architecture, interruption of fiber continuity around the hole, limited delamination in the same region, fiber crimp or directional deviation, bearing-induced local compliance losses, and resin microcracks reduce the measured stiffness. This, in turn, results in reduced reflection in the EI back-calculation. The trends in K and M within the same SCBP samples confirm that the material exhibits sufficient elastic response and load-carrying capacity. The problem stems from the effect of the geometry-hole-stacking triad in short clearances.

The results of the density normalization performed to isolate the mass effect are presented in Figure 7. As illustrated in Figures 7a–7c, the K/ρ, M/ρ, and EI/ρ ratios are shown, respectively. The densities of steel (ρ_{steel}) and carbon-fiber-reinforced plastic (CFRP) are 0.008 g/mm³ [40] and 0.001486 g/mm³, respectively. The density of CFRP was calculated from samples prepared with dimensions 50 × 50 × 4 mm and a mass of 14.86 g. For EI/ρ, SCBP ≈ 6.31×10^9 N.mm⁵/g and LCBP ≈ 4.27×10^9 N.mm⁵/g, versus steel groups ≈ 1.69×10^9 and ≈ 1.67×10^9 N.mm⁵/g, respectively. For K/ρ, SCBP ≈ 4.04×10^5, LCBP ≈ 1.20×10^5, and steel-long ≈ 4.72×10^4 N·mm²/g. For M/ρ, SCBP ≈ 2.92×10^7 N·mm⁴/g and LCBP ≈ 2.23×10^7 N·mm⁴/g, compared with steel-long ≈ 2.97×10^6 N·mm⁴/g. Thus, SCBP > LCBP ≫ steel with respect to K/ρ, M/ρ, and EI/ρ, thereby quantitatively confirming the stiffness-to-mass advantage of CFRP.

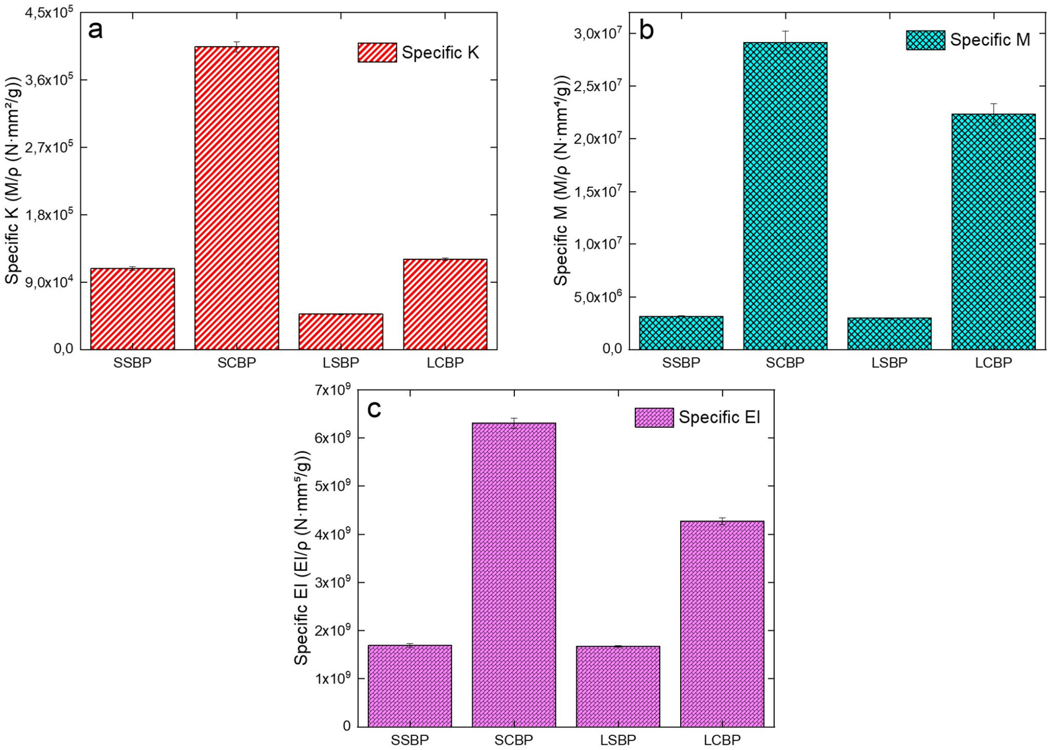

Figure 7. Four-point bending mass-normalized (specific) metrics, a) specific bending stiffness, b) specific moment, c) specific equivalent bending stiffness. Bars show mean ± SD (n = 3). Distinct letters denote significant differences at p 0.05

These visual findings were corroborated statistically: significant main effects of material (on K, M, and EI/ρ) and length (on K and M), and a significant material × length interaction for EI/ρ. Tukey HSD showed that both CFRP groups had higher values than both steel groups, and that SCBP had higher values than LCBP within CFRP (all $p < 0.05$). The intergroup differences (error bars) in Figures 6–7 provide a visual representation of these statistical outcomes. The reproducibility of the experiments in this study is high. For instance, the deviation for K is 2.08%; for short and long steel it is 1.50%; and for short and long CFRP it is 1.06% and 1.12%, respectively. For M, the respective values are 1.33%, 3.67%, 1.72%, and 4.55%. For EI, the values are 2.12%, 1.64%, 1.12%, and 1.59%, respectively. The low dispersion indicates that the differences forming the basis for interpretation are independent of sample noise.

From a design perspective, the findings of this study point to two clear conclusions. First, LCBP demonstrates superior performance relative to the reference LSBP, as evidenced by mass-normalized metrics (particularly EI/ρ). This outcome unequivocally substantiates the applicability of CFRP in contexts that prioritize lightness and stability. Secondly, SCBP exhibited the highest specific metrics (K/ρ, M/ρ, and EI/ρ) indicating that the mass-normalized advantage of CFRP is already pronounced in the short configuration. Nevertheless, fastener-region architecture (edge distance/spacing, hole-edge reinforcement, local fiber continuity, and edge finishing) remains a first-order design variable in safeguarding the absolute EI around holes. It is imperative to increase the hole spacing and edge distance to ensure that at least two screw pitches lie within the fixed-moment region. Furthermore, the implementation of local reinforcement around the hole is crucial. Maintaining 0° yarn continuity on the outer surface of plain-woven (0°/90°) fabrics is essential. Additionally, enhancing hole-edge finish and radius quality is vital to optimizing system performance. These interventions will allow an approach to the upper-limit behavior observed in LCBP in Figures 6d and 7c.

In summary, Figures 6–7 indicate that steel plates attain higher absolute stiffness, whereas CFRP plates are superior in specific (density-normalized) metrics. For CFRP, the short plate attains the highest specific values, while the long plate also surpasses both steel groups in specific values, despite exhibiting lower absolute bending stiffness, a result consistent with the long plate's extended span. These trends are corroborated by the reported group means (±SD) and the significance patterns depicted in Figures 6–7. Specifically, the short CFRP plate exhibited a reduction in absolute stiffness, which corresponded to the hole-region effects in laminated composites, such as net-section loss and local ply architecture. However, its efficiency advantage remained evident when normalized by mass. Collectively, these observations indicate that material selection significantly influences the equilibrium between absolute stiffness and stiffness efficiency when geometry is matched.

4. CONCLUSIONS

The present study compared 316L stainless steel and CFRP bone plates with identical geometry in four-point bending tests to determine whether CFRP can serve as a lower-mass alternative. The experimental findings indicate that steel plates exhibit higher absolute stiffness, whereas CFRP plates achieve superior specific stiffness. In the long plate, CFRP exhibited approximately 155% greater specific stiffness and approximately 651% greater specific bending moment than steel; in the short plate, the advantages were approximately 273% for specific stiffness and approximately 827% for specific bending moment. Conversely, steel exhibited higher absolute metrics: approximately 130% greater short absolute stiffness and 44% greater short bending stiffness, and approximately 235% greater long absolute stiffness and 111% greater long bending stiffness. In both short and long configurations, the lower absolute bending stiffness of CFRP relative to steel is explained by fiber interruptions at screw holes, local ply architecture, and hole-region fracture phenomena typical of laminated composites, rather than by an intrinsic weakness of the carbon-fiber material itself. Therefore, CFRP maintains a clear advantage in specific stiffness. Taken together, when the fastener region and working length are treated as primary design variables, CFRP can meet stability requirements with reduced mass. With geometry held constant and material densities normalized, the absolute and specific mechanical properties obtained for 316L steel and CFRP provide a design-oriented basis for material selection in weight-sensitive orthopedic applications.

5. REFERENCES

1. Mulinari-Santos, G., Paino Santana, A., Botacin, P.R. & Okamoto, R. (2024). Addressing the challenges in pediatric facial fractures: A narrative review of innovations in diagnosis and treatment. *Surgeries, 5*(4), 1130-1146.
2. Çetin, A. (2025). Use of sandwich structures in biomedical applications: an innovative design for external ring fixators. *Biomedical Materials, 20*(2), 025040.

3. Sen, D. (2022). Principles and overview of external fixators. *In: Banerjee, A., Biberthaler, P., Shanmugasundaram, S. (eds) Handbook of Orthopaedic Trauma Implantology. Springer*, Singapore.
4. Brouwer de Koning, S.G., de Winter, N., Moosabeiki, V., Mirzaali, M.J., Berenschot, A., Witbreuk, M.M.E.H. & Lagerburg, V. (2023). Design considerations for patient-specific bone fixation plates. *Medical & Biological Engineering & Computing, 61*(12), 3233-3252.
5. Augat, P. & von Rüden, C. (2018). Evolution of fracture treatment with bone plates. *Injury, 49*(1), 2-7.
6. Haase, K. (2009). *Finite element analysis of orthopaedic plates and screws and the effects of stress shielding.* University of Ottawa, Canada.
7. Zhang, S., Patel, D., Brady, M., Gambill, S., Theivendran, K., Deshmukh, S., Swadener, G., Junaid, S. & Leslie, L. (2022). Experimental testing of fracture fixation plates – a review. *Proceedings of the Institution of Mechanical Engineers, Part H: Journal of Engineering in Medicine, 236*(9), 1253-1272.
8. Galea, G.L. & Price, J.S. (2014). Four-point bending protocols to study the effects of dynamic strain. *In: Osteoporosis and Osteoarthritis*, *Springer,* 117-130.
9. Grassi, L. & Isaksson, H. (2015). Extracting accurate strain measurements in bone mechanics: A critical review of current methods. *Journal of the Mechanical Behavior of Biomedical Materials, 50*, 43-54.
10. Adanty, K. & Bhagavathula, K.B., Tronchin, O., Li, D.X., Nelson, K.N. (2023). The mechanical characterization and comparison of male and female calvaria under four-point bending impacts. *Journal of Biomechanical Engineering, 145*(5), 051009.
11. ASTM International, (2024). *Standard specification and test method for metallic bone plates (ASTM F382-24)*. ASTM International, West Conshohocken, PA, USA.
12. Strom, A.M., Garcia, T.C., Jandrey, K., Huber, M.L. & Stover, S.M. (2010). In vitro mechanical comparison of 2.0 and 2.4 limited-contact dynamic compression plates and 2.0 dynamic compression plates of different thicknesses. *Veterinary Surgery, 39*(7), 824-828.
13. Mariolani, J.R. & Belangero, W.D. (2013). Comparing the in vitro stiffness of straight-DCP, wave-DCP, and LCP bone plates for femoral osteosynthesis. *ISRN Orthopedics,* 308753.
14. Benli, S., Aksoy, S., Havıtcıoğlu, H. & Kucuk, M. (2008). Evaluation of bone plate with low-stiffness material in terms of stress distribution. *Journal of Biomechanics, 41*(15), 3229-3235.
15. Evans, A., Glyde, M., Day, R.E. & Hosgood, G. (2024). Effect of plate-bone distance and working length on 2.0-mm locking construct stiffness and plate strain in a diaphyseal fracture gap model: A biomechanical study. *Veterinary and Comparative Orthopaedics and Traumatology*, *37*(1), 1-7.
16. Mori, Y., Kamimura, M., Ito, K., Koguchi, M., Tanaka, H., Kurishima, H., Koyama, T., Mori, N., Masahashi, N. & Aizawa, T. (2024). A review of the impacts of implant stiffness on fracture healing. *Applied Sciences, 14*, 2259.
17. Ganesh, V.K., Ramakrishna, K. & Ghista, D.N. (2005). Biomechanics of bone-fracture fixation by stiffness-graded plates in comparison with stainless-steel plates. *BioMedical Engineering OnLine, 4*, 46.
18. Abdudeen, A., Abu Qudeiri, J.E., Kareem, A. & Valappil, A.K. (2022). Latest developments and insights of orthopedic implants in biomaterials using additive manufacturing technologies. *Journal of Manufacturing and Materials Processing, 6*(6), 162.
19. Eliaz, N. (2019). Corrosion of metallic biomaterials: A review. *Materials, 12*(3), 407.
20. Antunes, R.A. & de Oliveira, M.C.L. (2012). Corrosion fatigue of biomedical metallic alloys: Mechanisms and mitigation. *Acta Biomaterialia, 8*(3), 937-962.
21. Høl, P.J., Mølster, A. & Gjerdet, N.R. (2008). Should the galvanic combination of titanium and stainless steel surgical implants be avoided? *Injury, 39*(2), 161-169.
22. Geetha, M., Singh, A.K, Asokamani, R. & Gogia, A.K. (2009). Ti based biomaterials, the ultimate choice for orthopaedic implants – A review. *Progress in Materials Science, 54*(3), 397-425.
23. Radzi, S., Cowin, G., Robinson, M., Pratap, J., Volp, A., Schuetz, M.A. & Schmutz, B. (2014). Metal artifacts from titanium and steel screws in CT, 1.5T and 3T MR images of the tibial Pilon: a quantitative assessment in 3D. *Quantitative Imaging in Medicine and Surgery, 4*(3), 163-172.
24. Oğuz, Z.A. (2025). Assessment of the change in hardness of particulated intraply carbon/aramid reinforced composites after UV aging. *Çukurova Üniversitesi Mühendislik Fakültesi Dergisi, 40*(1), 219-226.
25. Yıldırım, S., Beylergil, B., Ergin, C.K. (2024). Investigation of the flexural performance of hybrid epoxy composites reinforced with nanosilica/sansevieria trifasciata (snake plant) natural fiber. *Çukurova Üniversitesi Mühendislik Fakültesi Dergisi, 39*(4), 1103-1112.
26. Bukvić, M., Milojević, S., Gajević, S., Đorđević, M. & Stojanović, B. (2025). Production technologies and application of polymer composites in engineering: A review. *Polymers*, *17*(16), 2187.

27. Georgantzinos, S.K., Giannopoulos, G.I., Stamoulis, K. & Markolefas, S. (2023). Composites in aerospace and mechanical engineering. *Materials, 16*(22), 7230.
28. Uzay, Ç. (2022). Mechanical and thermal characterization of laminar carbon/epoxy composites modified with magnesium oxide microparticles. *Polymer Composites*, *43*(1), 299-310.
29. Acer, D.C. & Geren, N. (2025). Stainless steel wire mesh hybridization for improved bending fatigue performance in fiber reinforced polymer sandwich structures. *Polymer Composites, 46*(3), 923-942.
30. Geren, N., Acer, D.C., Uzay, C. & Bayramoğlu, M. (2021). The effect of boron carbide additive on the low-velocity impact properties of low-density foam core composite sandwich structures. *Polymer Composites, 42*(4), 2037-2049.
31. Karaçor, B. & Özcanlı, M. (2021). Effect of various matrix materials on mechanical properties of basalt/jute/glass fiber reinforced hybrid composites. *Çukurova Üniversitesi Mühendislik Fakültesi Dergisi, 36*(4), 941-954.
32. Kurtz, S.M. & Devine, J.N. (2007). PEEK biomaterials in trauma, orthopedic, and spinal implants. *Biomaterials*, *28*(32), 4845-4869.
33. Chua, C.Y.X., Liu, H.C., Di Trani, N., Susnjar, A., Ho, J., Scorrano, G., Rhudy, J., Sizovs, A., Lolli, G., Hernandez, N., Nucci, M.C., Cicalo, R., Ferrari, M. & Grattoni, A. (2021). Carbon fiber reinforced polymers for implantable medical devices. *Biomaterials, 271*, 120719.
34. Arevalo, S., Arthurs, C., Echeverria Molina, M.I., Pruitt, L. & Roy, A. (2023). An overview of the tribological and mechanical properties of PEEK and CFR-PEEK for use in total joint replacements. *Journal of the Mechanical Behavior of Biomedical Materials, 145*, 105974.
35. Shiers-Gelalis, F., Giannoudis, V., Rodham, P. & Giannoudis, P.V. (2024). Surgeons' perspective on the use of carbon fibre plates for extremity fracture fixation. *European Journal of Orthopaedic Surgery & Traumatology, 35*(1), 26.
36. Giannoudis, V.P., Rodham, P., Antypas, A., Mofori, N., Chloros, G. & Giannoudis, P.V. (2023). Patient perspective on the use of carbon fibre plates for extremity fracture fixation. *European Journal of Orthopaedic Surgery & Traumatology, 33*(6), 2573-2577.
37. Rijs, Z., Weekhout, A., Daniel, S., Schoones, J. W., Groot, O.Q., Lozano-Calderon, S.A. & van de Sande, M.A.J. (2023). Carbon-fibre plates for traumatic and (impending) pathological fracture fixation: Where do we stand? A systematic review. *Journal of Orthopaedics and Traumatology, 24*(1), 42.
38. de Jong, J.J.A., Lataster, A., van Rietbergen, B., Arts, J.J., Geusens, P.P., van den Bergh, J.P.W. & Willems, P.C. (2017). Distal radius plate of CFR-PEEK has minimal effect compared to titanium plates on bone parameters in high-resolution peripheral quantitative computed tomography: A pilot study. *BMC Medical Imaging, 17*(1), 18.
39. ASTM International, (2024). *ASTM F382-24: Standard specification and test method for metallic bone plates.* ASTM International, West Conshohocken, PA, USA.
40. Shin, D.H., Seong, K.W., Nakajima, H.H., Puria, S. & Cho, J.H. (2020). A piezoelectric bellows round-window driver (PBRD) for middle-ear implants. *IEEE Access, 8,* 137947-137954.